Chemical imaging of single 4,7,12,15-tetrakis[2.2]paracyclophane by spatially resolved vibrational spectroscopy

N. Liu,[a] C. Silien,[b] and W. Ho[c]
Department of Physics and Astronomy, University of California, Irvine, California 92697-4575, USA and Department of Chemistry, University of California, Irvine, California 92697-4575, USA

J. B. Maddox and S. Mukamel
Department of Chemistry, University of California, Irvine, California 92697-4575, USA

B. Liu and G. C. Bazan
Department of Chemistry, University of California, Santa Barbara, California 93106-9510, USA

(Received 25 September 2007; accepted 29 October 2007; published online 28 December 2007)

Single 4,7,12,15-tetrakis[2.2]paracyclophane were deposited on NiAl(110) surface at 11 K. Two adsorbed species with large and small conductivities were detected by the scanning tunneling microscope (STM). Their vibrational properties were investigated by inelastic electron tunneling spectroscopy (IETS) with the STM. Five vibrational modes were observed for the species with the larger conductivity. The spatially resolved vibrational images for the modes show striking differences, depending on the coupling of the vibrations localized on different functional groups within the molecule to the electronic states of the molecule. The vibrational modes are assigned on the basis of *ab initio* calculations. No IETS signal is resolved from the species with the small conductivity. © *2007 American Institute of Physics*. [DOI: 10.1063/1.2815814]

I. INTRODUCTION

The demand for chemical characterization of heterogeneous systems at the nanometer scale is continuously growing due to its relevance in materials science, nanotechnology, pharmacology, and biochemistry. In this respect, optical imaging techniques with chemical selectivity such as fluorescence microscopy, infrared near-field scanning optical microscopy (IR NSOM), IR apertureless NSOM, and Raman scattering microscopy have been demonstrated and developed over the past years.[1–3] Microscopies with vibrational sensitivity can be used to measure the spatial distribution of particular functional groups. However, the information collected by these techniques is usually averaged over an ensemble of molecules and the spatial resolution is limited to tens of nanometers.

The scanning tunneling microscope (STM), however, provides the capability of resolving single molecules at the submolecular scale, and its chemical sensitivity is achieved by inelastic electron tunneling spectroscopy (IETS).[4] Spatially resolved vibrational intensity mapping makes it possible to image the distribution of a vibrational excitation within a single molecule. So far, the majority of the experiments were carried out on small molecules. However, it is important to demonstrate the ability of STM-IETS to study more complex molecules. The large molecules that have been studied by STM include single Cu(II) etioporphyrin-I,[5] C_{60}, C_{70},[6,7] and $Gd@C_{82}$.[8] Yet, only one vibrational mode was detected for the first three types of molecules. The lack of sensitivity of STM-IETS to some vibrational modes has been theoretically attributed to destructive interferences between inelastic and elastic channels.[9,10]

In this paper, we report on STM-IETS measurements conducted on single 4,7,12,15-tetrakis(4′-dimethylaminostyryl)[2,2]paracyclophane (DMAS-PCP) molecules adsorbed on NiAl(110) surface at 11 K. DMAS-PCP is a derivative of the distyrylbenzene dimers, which have been used as model systems for studying the ring stress, the intermolecular interactions, and the effects of through-space π-π delocalization on the photophysics of molecular aggregates.[11,12] Here, we focus our attention on the understanding of the interplay between the tunneling electron and the π-π stacking of the PCP core. For DMAS-PCP on NiAl(110), we observed two molecular states showing distinct topographic structures and conductivity. In one particular adsorption geometry, the molecule can be reversibly converted between these two states. IETS measurements obtained on these two species show strikingly different results. The state of smaller conductivity does not show any vibrational signal, while the one with the large conductivity exhibits rich vibrational features—five vibrational modes were detected in the spectrum. High-resolution IETS intensity images on the vibrational modes reveal different patterns, which are closely associated with the strength of the electron-phonon coupling to various functional groups within the molecule.

II. EXPERIMENTAL SECTION

All experiments were carried out at 11 K with a home-built variable temperature STM (Ref. 13) housed in an ultra-

[a]Present address: University of Alberta, Edmonton, T6G 2G7, Alberta, Canada.
[b]Present address: University of St. Andrews, North Haugh, St. Andrews, KY16 9ST, UK.
[c]Author to whom correspondence should be addressed. Electronic mail: wilsonho@uci.edu.

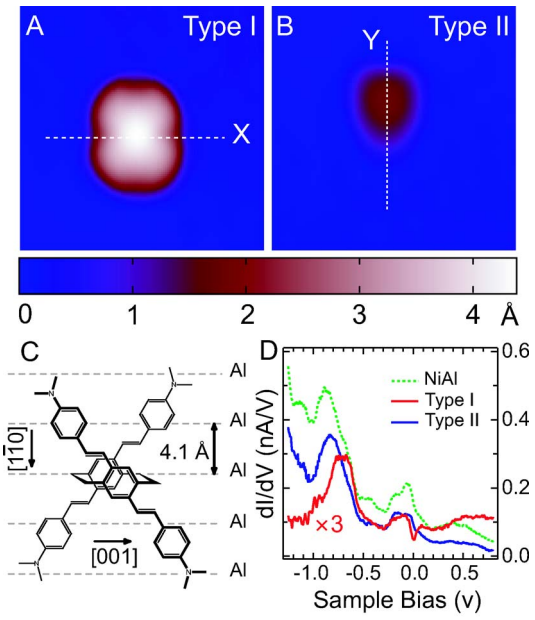

FIG. 1. (Color online) [(A) and (B)] STM topographies of four-lobed (type I) and pear shaped (type II) species on NiAl(110) at 11 K, size of 33 $\times 33$ Å^2, imaging condition of 0.1 nA tunneling current and 0.36 V sample bias. (C) Molecular structure of DMAS-PCP with respect to the NiAl(110) lattice for the four-lobed species. (D) dI/dV spectra for type I (red), type II (blue) molecules, and NiAl substrate (green), ranging from −1.2 to 0.8 V sample bias. The tunneling gap is set at 0.1 nA and −0.75 V for type II molecule, and 0.1 nA and 1.75 V for both type I molecule and NiAl substrate. The spectrum measured over type I molecule is amplified three times for clarity.

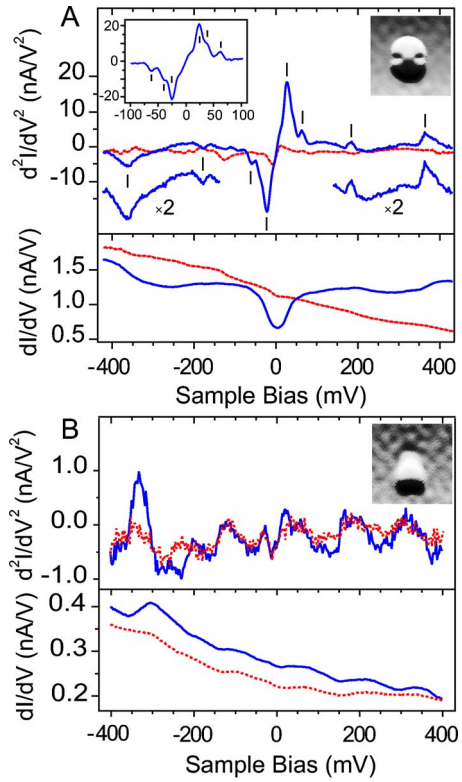

FIG. 2. (Color online) (A) d^2I/dV^2 and dI/dV spectra at the center of the type I molecule. The tunneling gap is set at 0.1 V and 0.1 nA. The full spectra are averaged over 50 passes, 4 min/pass, with 8 mV modulation. Spectrum shown as the inset is taken with 6 mV modulation. Spectra over NiAl(110) are taken at the same tunneling gap and are given in dashed curve for comparison. (B) d^2I/dV^2 and dI/dV spectra at the center of the type II molecule. Tunneling gap is set at −0.5 V and 0.18 nA. The spectra are averaged over 30 passes, 4 min/pass, with 8 mV modulation. Spectra over NiAl(110) are recorded at the tunneling gap of −0.4 V and 0.1 nA and are given in dashed curve for comparison. The illuminated images in the inset, size of 31×31 Å^2, were taken at 0.36 V, 0.25 nA.

high vacuum chamber (base pressure lower than 3×10^{-11} Torr). The NiAl(110) sample was prepared by repeated cycles of Ne^+ sputtering and annealing at 1300 K. The electrochemically etched polycrystalline Ag tips were cleaned by annealing before being transferred into the STM.

DMAS-PCP molecules were synthesized according to Ref. 12 and further purified by multiple thermal annealing in vacuum before use. They were evaporated onto the clean NiAl(110) surface at 11 K. The dI/dV and d^2I/dV^2 spectra were measured by a lock-in amplifier with ac modulation of the sample bias ranging from 6 to 15 mV at 264 Hz, while keeping the feedback loop open. The infrared spectrum was recorded with a JASCO FTIR 430 spectrometer by dispersing the DMAS-PCP crystals in KBr.

III. RESULTS AND DISCUSSION

The DMAS-PCP molecules adopt two distinct configurations on NiAl(110) at low temperature, as shown in Figs. 1(a) and 1(b). The apparent height of the four-lobed species (type I) is 4.4 Å above the surface, when imaged at 0.36 V and 0.1 nA. This species can only be observed when their X axis is aligned with the underlying Al rows (see Fig. 1). The pear shaped species (type II), about 2 Å above the surface, display several orientations, with the molecular axis Y in different angles with respect to the NiAl(110) lattice. Type II molecules make up the majority of the population. Only a small fraction of the total molecules ($\sim$10%) adopt the four-lobed configuration. Type I molecules can be reversibly converted to and from type II molecules with their Y axis aligned along the [1$\bar{1}$0] direction. This conversion is triggered by the electric field in the junction and tunneling electrons through the molecule. Detailed discussions of the switching mechanisms are given elsewhere.[14]

To gain information on the electronic and vibrational properties of the molecule, dI/dV and d^2I/dV^2 measurements were conducted at the center of both species (see Figs. 1 and 2). For type II molecules, no particular features can be extracted when comparing with the spectra recorded on the bare NiAl surface [Figs. 1(d) and 2(b)]. In contrast, the d^2I/dV^2 spectrum, acquired between −410 and 410 mV over the type I species, clearly shows five peaks and corresponding dips, at positive and negative sample biases, respectively (25, 40, 60, 179, and 365 mV). We attribute these characteristic inelastic channels to the excitations of molecular vibrations. Due to the resolution limit of STM-IETS, the vibrational mode at 40 mV only appears as a shoulder of the strong peak at 25 mV. It is better resolved with a smaller bias modulation (6 mV), as presented in the inset of Fig. 2(a). The full widths at half maximum of the 25, 60, and 179 mV peaks are similar and of about 19 mV, for a bias modulation of 8 mV. However, the peak around 365 mV is much broader, suggesting that multiple vibrational excita-

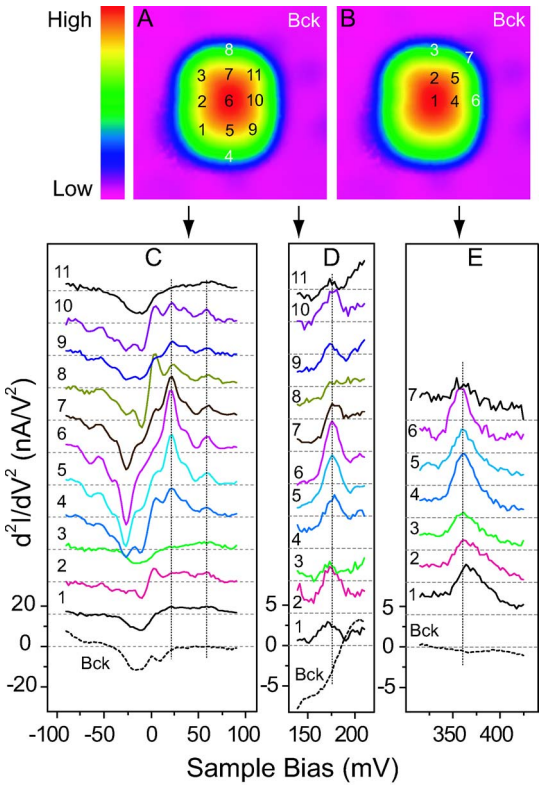

FIG. 3. (Color online) [(A) and (B)] STM topographies, size of 30 $\times$30 Å^2, imaging condition of 0.2 V and 0.1 nA. (C) d^2I/dV^2 spatial mapping. Tunneling gap set at 0.1 V, 0.1 nA. Each spectrum is averaged over 10 passes, 54 s/pass, 6 mV modulation. (D) d^2I/dV^2 spatial mapping. Tunneling gap set at 0.1 V, 0.1 nA. Each spectrum is averaged over 30 passes, 17 s/pass, 10 mV modulation. (E) d^2I/dV^2 spatial mapping. Tunneling gap set at 0.1 V, 0.1 nA. Spectra from point 1 to 7 are averaged over 70, 51, 50, 31, 63, 77, and 60 passes, respectively, 27 s/pass, 10 mV modulation.

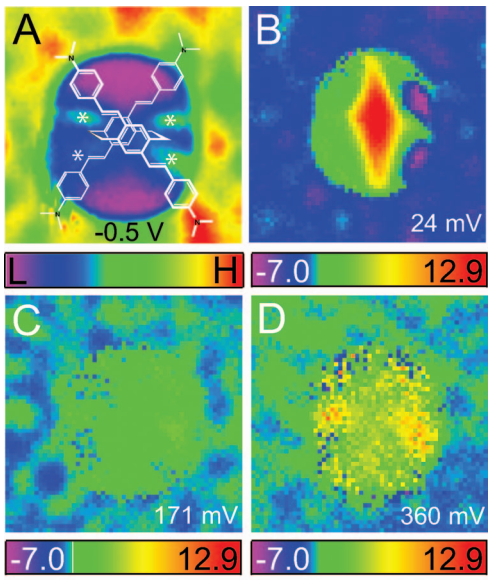

FIG. 4. (Color) (A) STM dI/dV microscopy, size of 30$\times$30 Å^2, tunneling gap set at 1.75 V, 0.1 nA. The dI/dV signal was acquired at −0.5 V, 15 mV ac modulation. "$*$" is used to denote the protrusions in the image. [(B)–(D)] STM d^2I/dV^2 microscopic images, size of 32$\times$32 Å^2. The tunneling gap was set at 0.1 V, 0.1 nA, and d^2I/dV^2 signal was recorded at 24 mV for (B), 171 mV for (C), and 360 mV for (D) with 15 mV ac modulation.

tions of similar energies are present.[15] The finer energy assignment is difficult to achieve due to resolution limitation.

The influence of the local environment of the molecule on the detection of the vibrational modes has been previously reported.[16] Here, our results highlight the effect of modifying the adsorption geometry of large molecules on the observation of vibrational inelastic channels. The existence of molecular electronic resonance close to the Fermi level is considered critical in obtaining appreciable signal from STM-IETS. This argument is strongly supported by theoretical computations carried out on small molecules.[9,10] For large molecules such as C_{60} and Gd at C_{82}, the interplay between the lowest unoccupied molecular orbital (LUMO) states and the detection of vibrational modes was also suggested.[6,8] Even though we do not know the exact adsorption geometry of type II species, the change in molecular adsorption configuration can be accompanied by variation of the relative positions of the atoms within the molecule and relative to the underlying NiAl lattice. Such a change can dramatically alter the energy and symmetry of the molecular orbitals. The large variation in the apparent height and shape of these two types of molecules leads us to believe that they possess very different electronic structures. This can account for the sharp contrast in the detection of vibrational excitations between these two species. The dI/dV spectra for both species and the bare NiAl surface, which are proportional to the local density of states (LDOS), are displayed in Fig. 1(d). Strong NiAl surface states at −0.85 V sample bias are observed. An occupied resonant state at −0.7 V is detected over the type I molecule. Even though we cannot conclude that this feature solely originates from the molecule, the energy shifting of the resonant states from that of the bare NiAl substrate suggests the presence of molecular electronic bands near the Fermi level, which leads to a change in the total DOS upon adsorption of the molecule.[17] The difference in symmetry between the two species could also play an important role in the lack of STM-IETS signal from the type II molecules. Theoretical calculations involving both the molecule and the NiAl substrate are needed to provide additional insight on the electronic structure of this system.

Recording d^2I/dV^2 spectra at various locations over a type I molecule allow us to visualize the spatial distribution of each vibrational mode. Three mappings are presented in Fig. 3. The d^2I/dV^2 microscopic images at 24, 171, and 360 mV were also acquired and are presented in Figs. 4(b)–4(d), respectively. The dI/dV image at −0.5 V is displayed in Fig. 4(a) for comparison. This image of the LDOS exhibits the same symmetry as the topography [Fig. 1(a)]. As shown in Fig. 1(d), the LDOS over the molecule, at −0.5 V, is relatively smaller than that of the NiAl surface when the tunneling gap is set at 1.75 V and 0.1 nA. Therefore, the area of lower intensity likely describes the physical location of the molecular skeleton, while the four protrusions close to the center (denoted by white "$*$" in the image) correspond to the empty space between the C–C bridging bonds of the PCP core and four dimethylaminostyryl groups [Fig. 1(c)]. The dI/dV images recorded at other voltages (from −1.25 to 0.75 V) all show similar patterns, implying that the same electronic bands dominate the conductance around the Fermi level.

The spatial distributions of the vibrational signal from type I molecules appear to be localized on some specific part of the molecule and are strongly mode dependent. The localization of IETS intensity has been previously observed for both small and large molecules and has been proposed theoretically that it bears a strong connection with the deformation rate of the electronic wave function subsequent to phonon displacements.[8,18] For C_{60} on Ag(110) and $Gd@C_{82}$ on Ag(001), the mode detected by STM-IETS is a vibration involving the entire fullerene cage. The d^2I/dV^2 images could be hardly related to any particular bonds within the molecule. However, in the case of Cu(II) etioporphyrin-I on Cu(001), vibrational images at the characteristic C–H stretch energy showed well localized signal, which allows the identification of the four methylene bridge C–H bonds inside the molecule. In our experiment, the lowest d^2I/dV^2 signal is systematically found over the four protruding areas, which is consistent with the physical empty space within the molecule. Dramatically different vibrational patterns are observed for different modes (see Fig. 4), suggesting that different functional groups couple to the inelastic tunneling electron with different strengths, depending on the vibration mode. By choosing the appropriate bias value and tip position, the coupling maximum can be tuned to particular function groups of the molecule.

Unlike electronic states, which are greatly broadened and shifted upon adsorption of the molecule, intramolecular vibrations are, in most cases, only slightly perturbed compared to their counterparts in gas phase. This assertion is usually even more pertinent for large molecules such as DMAS-PCP. Therefore, we have computed the normal modes of the isolated molecule in order to identify the groups of atoms that are involved the most in each of the vibrational modes detected by STM-IETS. Quantum chemistry calculations of the IR active modes are performed with a HF/6-31G(d) basis set and the resulting vibrational eigenenergies have been multiplied by 0.8929 to account for the typical overestimation of such computational method.[19,20] An infrared spectrum of DMAS-PCP crystals was also recorded. The infrared data and calculated IR spectrum are compared in Fig. 5(a). The agreement between the computed IR and experimental IR spectrum is sufficient such that the nature of nuclear motion can be qualitatively assigned. In order to pinpoint the vibrational modes detected in our STM-IETS measurements, the total change in the conductance ($\Delta\rho$), which is given by the sum of the elastic and inelastic contributions, is computed for all normal modes at HF/3-21G* level calculation.[8,18–21] The calculated vibrational eigenenergies are multiplied by 0.9085 to account for the frequency overestimation. The computed relative magnitude of $\Delta\rho$ and the measured IETS spectrum as a function of the vibrational energy are plotted in Fig. 5(b). It is clearly seen that only a few vibrational modes show appreciable $\Delta\rho$ values and that the calculations are in a fairly good agreement with the experimental observations. In the following discussion, only the vibrations with large computed $\Delta\rho$ are considered.

For smaller molecules, low frequency vibrational modes have been assigned to intermolecular vibrations, which involves bonding to the substrate.[16,22,23] However, for large molecules, such as DMAS-PCP, intermolecular modes are expected to be in the range of only a few millivolts.[24] We therefore believe the lowest energy mode observed in our spectrum to be still an intramolecular vibrational excitation. In the IETS mapping around 24 mV [Fig. 3(c)] it is clear that the strongest magnitude of the vibration stems from the center of the molecule (point 6). The corresponding vibrational image recorded at 24 mV [Fig. 4(b)] reveals that the signal is distributed in the shape of an elongated diamond and centered on the PCP core. The calculated low energy modes around 24 mV are characterized by out of plane C–C–N and C–C–C bending motions, distributed over the entire molecule. These motions result in subtle distortions in the paracyclophane skeleton, causing the parallel rings of the PCP core to oscillate between highly bent and flattened configurations. The calculations indicate that this vibrational mode is strongly coupled to the electronic density of the paracyclophane core of the molecule, in a good agreement with our spatially resolved vibration image. By positioning the tip right over the PCP core, the maximum IETS signals at low frequency can be selected.

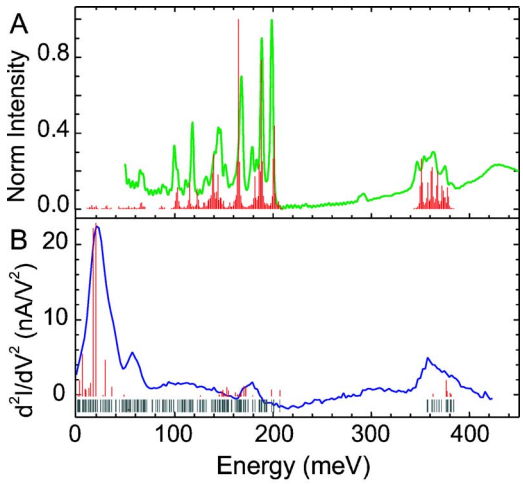

FIG. 5. (Color online) (A) Comparison of the experimental IR signal (green) and the calculated IR (red) intensities. (B) Comparison of the STM-IETS [blue, part of Fig. 2(a)] and the computed magnitude of the total change in conductance, indicated by the red lines. The gray lines at the bottom of the figure indicate the position of the computed normal mode frequencies.

The C–H stretches are the most frequently reported modes by STM-IETS and have been successfully used to identify specific functional groups within molecules previously.[5] The computed C–H modes include the C–H stretching motions located on the PCP bridges, styryl groups, and dimethylamino groups. The activation of multiple stretching modes results in the broad feature observed in the spectrum around C–H stretching region. The vibrational mapping at 360 mV [Fig. 4(d)] shows larger intensities at two opposite corners of the molecule, consistent with the IETS mapping shown in Fig. 3(e), where points 4 and 6 display the largest amplitudes. Given the structure of DMAS-PCP [Fig. 1(c)], we attribute this IETS signal to C–H stretch motions in the CH_2 groups localized on the C–C bonds bridging the PCP core.

The vibrational image recorded at 171 mV exhibits relatively small magnitude variations over the entire physical

area of the molecule. The calculation shows several modes possibly accounting for this vibrational resonance. They mostly involve the in-plane C–C–H bending throughout the molecule. An asymmetric character is observed in Fig. 4(c) and is clearly illustrated in the IETS mapping shown in Fig. 3(d). For example, at 171 mV, the d^2I/dV^2 values at the points 3 and 11 are −1.9 and +0.84 $\mathrm{nA/V^2}$, respectively. The peaks associated with the vibrational mode are, however, similar in width and intensity at these two points when the background signal is taken into account. This asymmetry is expected to result from the unevenness of the electronic states of the underlying NiAl(110) surface. It is also observed on the vibrational images and mappings at other vibration energies.

The NiAl(110) substrate plays a crucial role in realizing and stabilizing type I molecules, as this configuration is only observed for the orientation of the *X* axis of the molecule aligned along the [001] direction of NiAl and since only type II species were found when using Cu(111) as substrate. Calculations of the hybridized molecular electronic structure with the NiAl(110) surface should provide deeper insights on the adsorption geometry of the two stable molecular states, conversion mechanism, as well as the lack of IETS signal for type II species.

IV. CONCLUSION

Two distinct adsorbate states were observed for DMAS-PCP molecules deposited on NiAl(110) at 11 K. The STM-IETS measurements on these two species show striking differences, which are attributed to differences in the adsorbate symmetry and molecular electronic states of the two species. The NiAl(110) lattice plays a critical role in stabilizing the four-lobed molecular state, hence the detection of the vibrational modes. By recording the vibrational intensity images for each energy mode, the spatial distribution of the different modes can be visualized. These images partially resemble the symmetry of the molecule, while images at 24 and 360 mV show additional characteristic patterns that are closely related to particular functional groups. The distinct patterns make it possible to selectively excite different vibrational modes. Our experiment demonstrates the use of STM-IETS as a technique to differentiate and selectively excite vibrational modes localized on different functional groups within a molecule.

ACKNOWLEDGMENTS

This work has been supported by the National Science Foundation, Chemical Bonding Center, Grant No. CHE-0533162. In addition, S.M. and G.C.B. gratefully acknowledge the support of NSF-NIRT Grant No. ECC-040675C and W.H., the Air Force Office of Scientific Research, Grant No. FA9550-04-10181. C.S. was a Scientific Research Worker of the Belgian National Funds for Scientific Research (FNRS).

[1] E. Betzig and J. K. Trautman, Science **257**, 189 (1992).
[2] M. Hashimoto and T. Araki, Opt. Lett. **25**, 1768 (2000).
[3] A. Volkmer, J. X. Cheng, and X. S. Xie, Phys. Rev. Lett. **87**, 023901 (2001).
[4] B. C. Stipe, M. A. Rezaei, and W. Ho, Science **280**, 1732 (1998).
[5] T. M. Wallis, X. Chen, and W. Ho, J. Chem. Phys. **113**, 4837 (2000).
[6] J. I. Pascual, J. Gómez-Herrero, D. Sáchez-Portal, and H. P. Rust, J. Chem. Phys. **117**, 9531 (2002).
[7] N. Liu, N. A. Pradhan, and W. Ho, J. Chem. Phys. **120**, 11371 (2004).
[8] M. Grobis, K. H. Khoo, R. Yamachika, X. Lu, K. Nagaoka, S. G. Louie, M. F. Cormmie, H. Kato, and H. Shinohara, Phys. Rev. Lett. **94**, 136802 (2005).
[9] N. Lorente, Appl. Phys. A: Mater. Sci. Process. **78**, 799 (2004).
[10] N. Mingo and K. Makoshi, Phys. Rev. Lett. **84**, 3694 (2000).
[11] S. Wang, G. C. Bazan, S. Tretiak, and S. Mukamel, J. Am. Chem. Soc. **122**, 1289 (2000).
[12] G. P. Bartholomew and G. C. Bazan, J. Am. Chem. Soc. **124**, 5183 (2002).
[13] B. C. Stipe, M. A. Rezaei, and W. Ho, Rev. Sci. Instrum. **70**, 137 (1999).
[14] C. Silien, N. Liu, W. Ho, J. B. Maddox, S. Mukamel, B. Liu, and G. C. Bazan, Nano Lett. (in press, 2007).
[15] L. J. Lauhon and W. Ho, J. Phys. Chem. A **104**, 2463 (2000).
[16] J. I. Pascual, J. J. Jackiw, Z. Song, P. S. Weiss, H. Conrad, and H. P. Rust, Phys. Rev. Lett. **86**, 1050 (2001).
[17] K. H. Hansen, J. Gottschalck, L. Petersen, B. Hammer, E. Lægsgaard, F. Besenbacher, and I. Stensgaard, Phys. Rev. B **63**, 115421 (2001).
[18] N. Lorente and M. Persson, Phys. Rev. Lett. **85**, 2997 (2000).
[19] M. J. Frisch, G. W. Trucks, H. B. Schlegel *et al.*, GAUSSIAN 03, Revision C.02, Gaussian, Inc., Wallingford, CT, 2004.
[20] J. B. Foresman and A. Frisch, *Exploring Chemistry with Electronic Structure Methods* (Gaussian, Pittsburgh, 1996).
[21] Following a procedure similar to that stated in Refs. 8 and 18, the estimation of the change in conductance is reduced to compute the electron-phonon coupling matrix elements with a scaling factor related to the vibration frequency. We invoke a phenomenological broadening of the molecular orbital eigenspectrum, where the energy levels are assumed to take a Lorentzian form. The broadening parameter Γ is chosen to be 0.025 eV and the Fermi level of the molecule is taken to be at the LUMO energy to give the best qualitative agreement between calculated and observed IET resonances.
[22] L. J. Lauhon and W. Ho, Phys. Rev. B **60**, R8525 (1999).
[23] J. R. Hahn, H. J. Lee, and W. Ho, Phys. Rev. Lett. **85**, 1914 (2000).
[24] H. Park, J. Park, A. K. L. Lim, E. H. Anderson, A. P. Alivisatos, and P. L. McEuen, Nature (London) **407**, 57 (2000).